nature nanotechnology

FOCUS | LETTERS

PUBLISHED ONLINE: 23 FEBRUARY 2015 | DOI: 10.1038/NNANO.2014.324

Domain-wall velocities of up to 750 m s^{-1} driven by exchange-coupling torque in synthetic antiferromagnets

See-Hun Yang†, Kwang-Su Ryu† and Stuart Parkin*

The operation of racetrack memories[1–3] is based on the motion of domain walls in atomically thin, perpendicularly magnetized nanowires, which are interfaced with adjacent metal layers with high spin–orbit coupling. Such domain walls have a chiral Néel structure[4–7] and can be moved efficiently by electrical currents[5,6]. High-capacity racetrack memory requires closely packed domain walls, but their density is limited by dipolar coupling from their fringing magnetic fields[3]. These fields can be eliminated using a synthetic antiferromagnetic structure composed of two magnetic sub-layers, exchange-coupled via an ultrathin antiferromagnetic-coupling spacer layer[8]. Here, we show that nanosecond-long current pulses can move domain walls in synthetic antiferromagnetic racetracks that have almost zero net magnetization. The domain walls can be moved even more efficiently and at much higher speeds (up to ~750 m s^{-1}) compared with similar racetracks in which the sub-layers are coupled ferromagnetically. This is due to a stabilization of the Néel domain wall structure, and an exchange coupling torque that is directly proportional to the strength of the antiferromagnetic exchange coupling between the two sub-layers. Moreover, the dependence of the wall velocity on the magnetic field applied along the nanowire is distinct from that of the single-layer racetrack due to the exchange coupling torque. The high domain wall velocities in racetracks that have no net magnetization allow for densely packed yet highly efficient domain-wall-based spintronics.

The manipulation of magnetization using torques derived from spin-polarized currents[3,9] and spin–orbit coupling phenomena[10] allow entirely novel magnetic memory and logic devices to be created. These are based on the switching of the magnetization of individual magnetic nano-elements, such as the moment of a magnetic tunnel junction (the direction of which encodes the state of the memory[11]) or, alternatively, on the spatial positioning or presence or absence of domain walls (DWs) in magnetic racetracks[12]. The latter option, in the form of a current-controlled DW shift register (namely, a racetrack memory), has been proposed as an innately three-dimensional memory-storage device with a potential density rivalling that of magnetic disk drives but with the performance and endurance of solid-state memories[2,3]. One major roadblock to the development of racetrack memory is the density of packing of the DW memory bits along the magnetic nanowires that form the racetracks. This packing density is limited by magnetic dipole fringing fields from the racetrack, which give rise to interactions between the DWs. These fringing fields can be largely eliminated by forming the racetracks from artificial antiferromagnetic structures that rely on long-range oscillatory interlayer exchange coupling via ultrathin metallic layers[13,14]. Such synthetic antiferromagnetic (SAF) structures are key to the successful operation of magnetic recording read heads as well as spin-transfer-torque magnetic random access memory[8].

Here, we show that DWs can be moved by current in SAF racetracks formed from two perpendicularly magnetized Co|Ni multilayers separated by an ultrathin antiferromagnetic (AF) coupling layer of Ru. We show that this is possible in SAF structures in which the spin transfer torque is derived predominantly from either conventional volume spin-dependent scattering[9] or from interfacial chiral spin torques[5,6]. In the former, in which the DWs move slowly and in the direction of electron flow, we find that the DW velocity in the SAF structure is comparable to that in similar synthetic ferromagnetic (SF) structures in which the Ru spacer thickness is slightly adjusted to allow for ferromagnetic (F) coupling of the two layers. In the latter, we find a dramatic enhancement of DW velocity in the SAF compared to that in the SF structure and, furthermore, that the DW velocity increases monotonically as the net magnetization of the SAF structure is decreased.

The samples have structures formed from a lower magnetic layer (LM) of thickness t_L (3 Co|7 Ni|1.5 Co), coupled via a Ru layer of thickness t_{Ru} to an upper magnetic layer (UM) of thickness t_U (t_a Co|7 Ni|t_b Co), where t_a and t_b are either 1.5 or 3Å (all thicknesses throughout this Letter are given in ångstroms). The LM and UM display perpendicular magnetic anisotropy with square hysteresis loops with a remanent magnetization equal to the saturation magnetization. Magnetic wires (2 μm wide and 50 μm long) were fabricated by photolithography and argon ion milling. Polar Kerr microscopy was used to image the motion of DWs along the wires in response to sequences of current pulses with lengths varying from 2.5 to 25 ns (refs 5, 15). Results are shown in Fig. 1a,b for typical SF and SAF wires, respectively.

When the Co|Ni|Co films are deposited on Pt underlayers, the DWs have a chiral Néel structure due to a Dzyaloshinskii–Moriya exchange interaction (DMI)[16–20] derived from strong spin–orbit coupling and the proximity-induced moment in Pt[6]. Schematic diagrams of the DW structure are presented in Fig. 1c,d for the SF and SAF nanowires, respectively. The magnetization rotates from up (↑) to down (↓) anticlockwise in a plane parallel to the length of the nanowire such that the magnetization in the middle of the DW (M_L) is aligned along the nanowire. When the exchange coupling between the LM and UM layers is sufficiently strong, the DW in the UM layer has the same chirality as that in the LM, irrespective of whether the coupling is F or AF (see Supplementary Discussion 1 for more details). Thus, for the SAF case, the moment in the middle of the ↓↑ DW in the UM (M_U) will be aligned in the opposite direction to that in the LM. As illustrated schematically in Fig. 1e,f, when current flows through the

Magnetoelectronics, IBM Almaden Research Center, San Jose, California 95120, USA. †These authors contributed equally to this work.
*e-mail: stuart.parkin@us.ibm.com

NATURE NANOTECHNOLOGY DOI: 10.1038/NNANO.2014.324

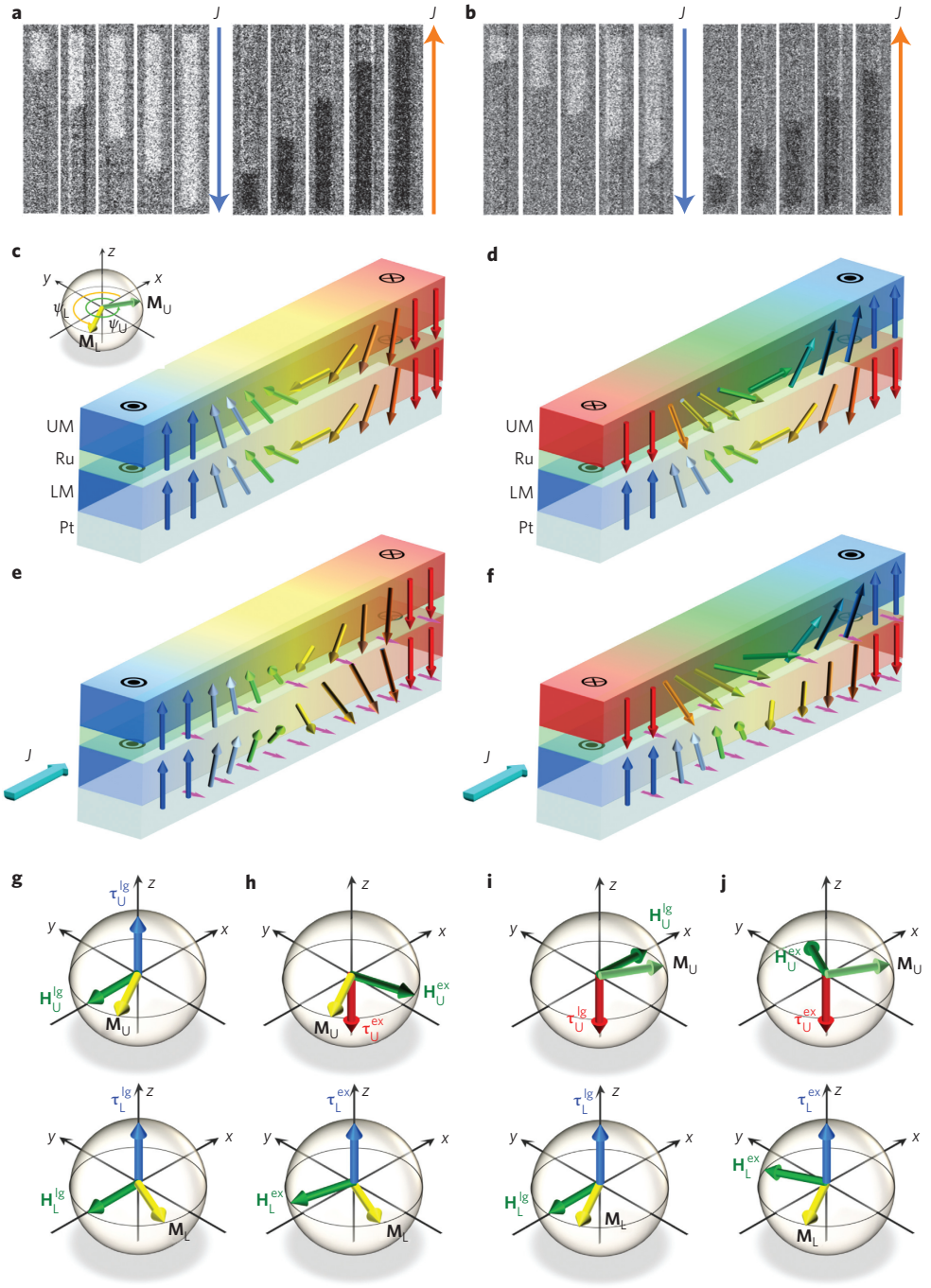

Figure 1 | Current-driven DW motion in SAF and SF nanowires: experiment and schematic illustration of torques. a,b, Kerr microscope images of a single DW moving along a nanowire formed from 20 TaN|15 Pt|3 Co|7 Ni|1.5 Co|t_{Ru} Ru|1.5 Co|7 Ni|1.5 Co|50 TaN with $t_{Ru} = 2$ (SF) (**a**) and $t_{Ru} = 8$ (SAF) (**b**). Each image (left to right) is taken after applying a train of current pulses (current density $J \approx 3.0 \times 10^8$ A cm^{-2}; see Supplementary Discussion 4) composed of 4×5 ns (**a**) and 2×5 ns (**b**) pulses. Blue and orange arrows represent the direction of current flow over the 100 ns integrated pulse time span. Light and dark contrast corresponds to ↑ and ↓ magnetization directions, respectively. **c**–**f**, Schematic illustrations of DWs in the upper (UM) and lower (LM) magnetic layers in perpendicularly magnetized SF (**c**,**e**) and SAF (**d**,**f**) nanowires for $J = 0$ (**c**,**d**) and finite J (**e**,**f**). Inset in **c**: DW angles ψ_L and ψ_U of DW magnetization of M_L (lower layer) and M_U (upper layer), respectively. M_L and M_U are the magnetizations in the centre of the DWs in the UM and LM, respectively, and exhibit an anticlockwise Néel structure when $J = 0$. When $J \neq 0$, M_L and M_U are rotated towards the spin accumulation direction denoted by the magenta arrows and are subjected to longitudinal fields H_L^{lg} and H_U^{lg}, respectively, which are composed of the corresponding DMI fields and H_x, and exchange-coupling fields H_L^{ex} and H_U^{ex}, respectively. Each of these fields gives rise to a corresponding torque, namely τ_L^{lg} and τ_U^{lg}, and τ_L^{ex} and τ_U^{ex}. **g**–**j**, Directions of fields and torques shown schematically for the SF case (**g**,**h**) and the SAF case (**i**,**j**). In each panel, upper and lower diagrams correspond to UM and LM, respectively. All thicknesses are in ångströms.

nanowire, the spin current generated by the spin Hall effect[21,22] in the Pt layer[23] induces a torque on the DW in the LM that results in rotation of the magnetization of the DW towards the accumulated spin direction transverse to the length of the nanowire. It is predominantly this spin Hall torque (SHT) in conjunction with the DMI field torque that results in motion of the DW

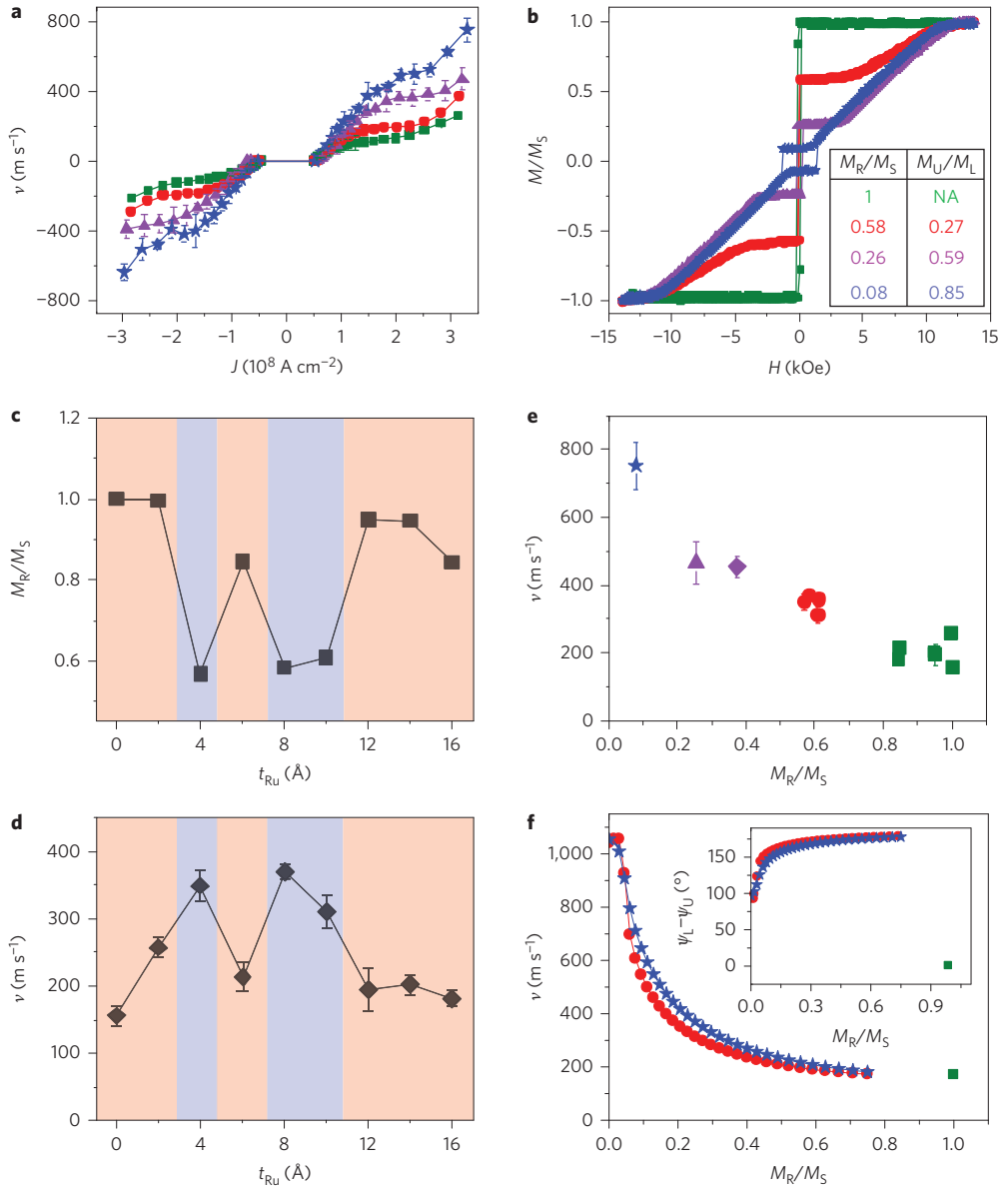

Figure 2 | Influence of SF and SAF structure on DW velocity. a,**b**, DW velocity v as a function of current pulse density J (**a**) and normalized perpendicular magnetization versus field hysteresis loops measured by a polar Kerr magnetometer (**b**) in nanowires formed from 20 TaN|15 Pt|3 Co|7 Ni|1.5 Co|t_{Ru} Ru|t_a Co|7 Ni|t_b Co|50 TaN, where $t_{Ru} = 2$, $t_a = 1.5$, $t_b = 1.5$ (green squares), $t_{Ru} = 8$, $t_a = 1.5$, $t_b = 1.5$ (red circles), $t_{Ru} = 8$, $t_a = 3$, $t_b = 1.5$ (violet triangles) and $t_{Ru} = 8$, $t_a = 3$, $t_b = 3$ (blue stars). Inset table (**b**): M_R/M_S and M_U/M_L values obtained from the corresponding colour-coded hysteresis loops in the main panel. **c**,**d**, M_R/M_S ratio (**c**) and DW velocity v (**d**) as a function of t_{Ru} for 20 TaN|15 Pt|3 Co|7 Ni|1.5 Co|t_{Ru} Ru|1.5 Co|7 Ni|1.5 Co|50 TaN. Orange and blue shaded regions correspond to SF ($J^{ex} > 0$) and SAF ($J^{ex} < 0$), respectively. **e**, Dependence of measured DW velocity v on M_R/M_S for nanowires formed from 3 Co|7 Ni|1.5 Co|0, 2, 6, 12, 16 Ru|1.5 Co|7 Ni|1.5 Co (green squares, SF); 3 Co|7 Ni|1.5 Co|4, 8, 10 Ru|1.5 Co|7 Ni|1.5 Co (red circles, SAF); 3 Co|7 Ni|1.5 Co|8 Ru|1.5 Co|7 Ni|3 Co (violet diamond, SAF); 3 Co|7 Ni|1.5 Co|8 Ru|3 Co|7 Ni|1.5 Co (violet triangle, SAF); 3 Co|7 Ni|1.5 Co|8 Ru|3 Co|7 Ni|3 Co (blue star, SAF); each with 20 TaN|15 Pt underlayer and 50 TaN capping layer. **f**, Calculated DW velocity and ψ_L-ψ_U (inset) versus M_R/M_S within the 1D model for SF (green square, $J^{ex} = 0.5$ erg cm^{-2}) and SAF (red circles and blue stars, $J^{ex} = -0.5$ erg cm^{-2}) nanowires. Parameters used in the model for a ↑↓ DW in LM (see Supplementary Discussion 1 for definitions) are $\Delta = 4.3$ nm, $u_L = u_U = 60$ m s^{-1}, $\alpha_L = \alpha_U = 0.1$, $\beta_L = \beta_U = 0$, $H_L^k = H_U^k = 1,400$ Oe, $H_L^{SH} = 1,650$ Oe and $H_L^{SH} = 500$ Oe, $H_L^{DM} = -1,400$ Oe, $H_L^{DM} = -300$ Oe (green square, SF), 300 Oe (red circles, SAF) and 800 Oe (blue stars, SAF). Error bars in **a**, **d** and **e** correspond to one standard deviation. All thicknesses are in ångströms.

in the direction of the current along the nanowire[5,6,20,24]. The magnitude of the spin Hall torque depends on the angle between M_L (or M_U) and the spin accumulation direction. As the current is increased, M_L (or M_U) rotates towards the spin accumulation direction so that eventually a Bloch DW structure results in which M_L (or M_U) is oriented transverse to the nanowire and the spin Hall torque becomes zero. As a result, the DW velocity becomes saturated with increasing current. Here, we show that the SAF structure stabilizes the Néel DW structure, thereby allowing much larger spin–orbit torques for the same current density, and therefore higher DW velocities. However, in addition, the SAF structure gives rise to a novel torque associated with the AF exchange coupling field. This exchange coupling torque (ECT) is about one order of magnitude larger than the DMI field torque and is key to accounting for the much higher DW velocities in the SAF racetracks.

The dependence of DW velocity v on current density is compared in Fig. 2a for several nanowires formed from structures that are identical except that the Ru thickness is slightly changed from 2Å to 8Å to allow for F or AF coupling[13]. The corresponding perpendicular magnetization versus field hysteresis loops are shown in Fig. 2b. For the SF case the hysteresis loop is square when the remanent magnetization M_R is equal to the saturation magnetization M_S. For the SAF structures $M_R \equiv |M_L - M_U|$, $M_S \equiv |M_L + M_U|$ and a significant field (up to ~1.2T in Fig. 2b, determined by the strength of the AF coupling) is required to saturate the magnetization (see Supplementary Discussion 3 for more details). It is clear from Fig. 2a that the DW velocity is significantly higher for the SAF structures than for the SF structure. Moreover, as the magnetization of the UM is increased to more closely compensate for that of the LM, the DW velocity increases monotonically, reaching a value of value of ~750 m s^{-1} when $M_U/M_L \approx 0.85$.

The relationship of the DW velocity with M_R/M_S is shown in Fig. 2c,d for a series of nearly identical samples in which only the Ru layer thickness t_{Ru} is varied. Clearly, the SAF structures sustain significantly higher DW velocities than the SF structures. The detailed dependence of v on M_R/M_S is shown in Fig. 2e for a series of AF coupled samples ($t_{Ru} = 8$ Å), each with an identical LM but where the UM is varied. As M_R/M_S is decreased from 1 (F coupling), v increases and attains a velocity of almost 800 m s^{-1} when $M_R/M_S = 0.08$, which is more than four times higher than the velocity for the F coupled racetracks and more than two times higher than the highest current-induced DW velocity yet reported in any racetrack[5,25].

Considerable insight into why DWs can move much faster under chiral spin torque in SAF than in SF structures is obtained by developing a one-dimensional (1D) model of the magnetization dynamics. The 1D model assumes that the DW profile remains unchanged during the current- and field-induced motion of the DWs[26]. The motion of the DWs in each magnetic sub-layer can be described by two parameters, their position q_i (i = L or U) along the nanowire and the angle ψ_i by which M_L or M_U is rotated within the plane of the wire from the x axis oriented along the wire (see Fig. 1). Independent Landau–Lifshitz–Gilbert equations for each sub-layer are coupled by AF or F exchange coupling via the Ru spacer layer. We assume that this coupling is sufficiently large that the DWs in each sub-layer are locked into position so that $q = q_L = q_U$. These equations are solved to find stationary solutions of ψ_i under given current and field conditions.

The spin Hall torque generated in the Pt underlayer results in both M_L and M_U rotating towards the transverse direction, $-y$ (along the spin accumulation), although the spin current intensity in the UM will be attenuated through the thickness of the LM and the Ru layer (with attenuation lengths estimated to be ~1 nm (refs 27–29) and 4 nm (ref. 30), respectively; see Fig. 1e,f). Once M_L and M_U are rotated from their equilibrium conditions they will be subjected to several torques that include a longitudinal field torque τ_i^{lg}, derived from the DMI field (and any longitudinal field H_x that might be applied, as discussed later), a damping torque that is proportional to the time derivative of M_L or M_U, and an anisotropy field-derived torque[5]. For the SAF and SF cases there is an additional torque (τ_L^{ex} and τ_U^{ex}) derived from the exchange coupling fields (H_L^{ex} and H_U^{ex}). All these torques are directed along the z axis and therefore contribute to the motion of the DW, but the damping and anisotropy field torque are small. The largest torques are the exchange coupling torque (Fig. 1h,j) and the DMI torque (Fig. 1g,i), but the former is much larger in the samples studied here because the exchange coupling field is much larger than the DMI field. However, because the sign of the exchange coupling torque is opposite for the upper and lower layers in both the SF and SAF cases, the torques drive the DWs in the upper and lower layers in opposite directions in the SF case so that there is no net driving force for the composite DW (Fig. 1h). By contrast, in the SAF case, these torques correspondingly drive the DWs in the upper and lower layers in the same direction and thereby provide a powerful novel driving mechanism for the composite DW (Fig. 1j and Supplementary Discussions 1 and 2). The exchange coupling

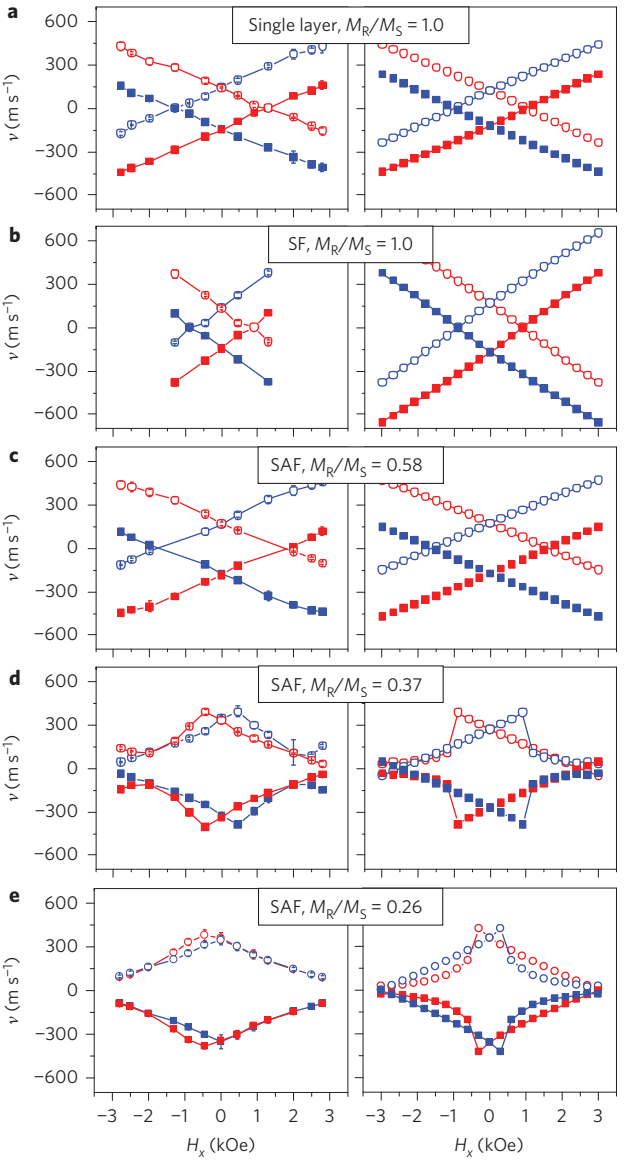

Figure 3 | Longitudinal field dependence of DW velocity for SF and SAF structures. a–e, Left and right panels: measured and calculated (1D model) DW velocities versus strength of applied longitudinal field H_x for nanowires formed from a single magnetic layer (**a**), an SF structure (**b**) and SAF nanowires (**c–e**) with different values of M_R/M_S. The structures are as follows: 3 Co|7 Ni|1.5 Co|50 Ru (**a**); 3 Co|7 Ni|1.5 Co|2 Ru|1.5 Co|7 Ni|1.5 Co|50 TaN (**b**); 3 Co|7 Ni|1.5 Co|8 Ru|1.5 Co|7 Ni|1.5 Co|50 TaN (**c**); 3 Co|7 Ni|1.5 Co|8 Ru|1.5 Co|7 Ni|3 Co|50 TaN (**d**); 3 Co|7 Ni|1.5 Co|8 Ru|3 Co|7 Ni|1.5 Co|50 TaN (**e**). Each has a 20 TaN|15 Pt underlayer. $J = 2.5 \times 10^8$ A cm^{-2} with 5 ns long current pulses. Red and blue symbols correspond to ↑↓ and ↓↑ domain configurations, respectively. Open and filled symbols correspond to positive and negative currents, respectively. The fitting parameters used are summarized in Supplementary Table 1. Open and filled symbols correspond to positive (+x) and negative (−x) current directions, respectively. Error bars shown in the left panels of **a–e** correspond to one standard deviation. All thicknesses are in ångströms.

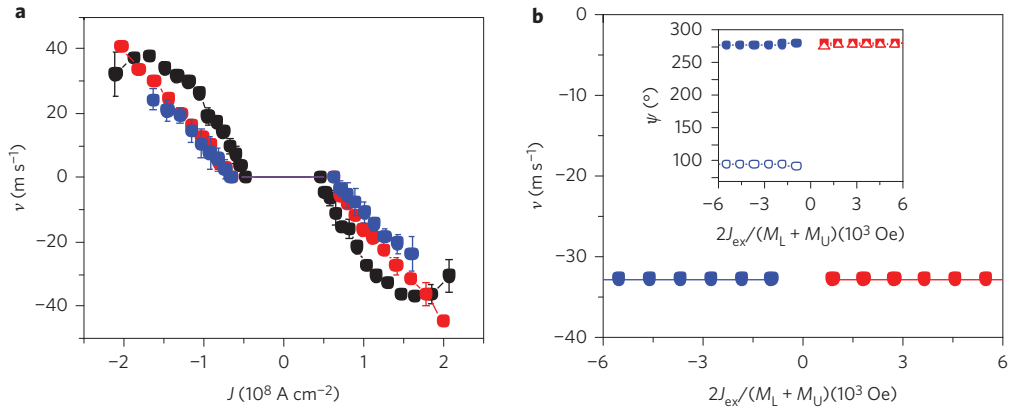

Figure 4 | Current-driven DW dynamics in nanowires formed on Au underlayers. a, Measured DW velocity v versus current density J for nanowires formed from a single layer (black), SF structure (red) and SAF structure (blue). Detailed structures: 3 Co|7 Ni|3 Co|7 Ni|1.5 Co (black), 3 Co|7 Ni|1.5 Co|2 Ru|1.5 Co|7 Ni|1.5 Co (red) and 3 Co|7 Ni|1.5 Co|8 Ru|1.5 Co|7 Ni|1.5 Co (blue), each with a 50 Ta|30 Au underlayer and capped with 50 TaN. **b**, DW velocity calculated using the 1D model versus $2J^{ex}/(M_L + M_U)$, where J^{ex} is the exchange coupling constant (see Supplementary Discussion 1 for details). Red and blue symbols correspond to SF and SAF structures, respectively. Parameters used in the model (for a ↑↓ DW in LM) are $\Delta = 8.5$ nm, $u_L = u_U = 41$ m s^{-1}, $\alpha_L = \alpha_U = 0.1$, $\beta_L = \beta_U = 0.08$, $H_L^k = H_U^k = 800$ Oe, $H_L^{SH} = H_U^{SH} = 0$, $H_L^{DM} = 300$ Oe, $H_U^{DM} = \pm 300$ Oe (+, SAF; –, SF), $M_L = 6 \times 10^{-5}$ emu cm^{-2}, $M_U = 4.2 \times 10^{-5}$ emu cm^{-2}. ψ_L (filled symbols) and ψ_U (open symbols) are plotted in the inset. Error bars in **a** correspond to one standard deviation. All thicknesses are in ångströms.

torque readily accounts for the dependence of the DW velocity on the degree of compensation of the SAF structure, as shown in Fig. 2f. These data are calculated using experimentally derived properties of the Co|Ni nanowires and are in excellent agreement with our experimental data (Fig. 2e). We note that the exchange coupling torque is maximized when $\psi_L - \psi_U = 90°$ during the current-induced motion of the DWs (Fig. 2f inset and Supplementary Discussion 2). The model shows that for a perfectly compensated SAF the DW velocity exceeds 1,000 m s^{-1}.

To understand the origin of the higher DW velocities in the SAF structures we compare in Fig. 3 the dependence of v on H_x, a longitudinal magnetic field applied along the nanowire for various racetracks. We have previously shown that for single-layer racetracks (Fig. 3a) the DW velocity goes to zero at a special value of H_x that is largely independent of the driving current, and takes opposite signs for the ↓↑ and ↑↓ DW configurations. This field reflects the internal magnetic exchange field to which the DWs are subjected and which is considered to be derived from DMI[5,20,24]. This interaction results in the DWs exhibiting a chiral Néel structure where the chirality is determined by the interface of the magnetic layer with the underlayer metal[6]. As shown in Fig. 3b, the SF racetracks obtained with thin Ru layers that give rise to F coupling show an almost identical behaviour to the single-layer racetracks. Depending on the DW configuration, for a given chirality the Néel structure is either stabilized by H_x and the DWs go faster, or the Néel structure is destabilized by H_x and the DWs slow down. This corresponds to whether H_x is parallel or antiparallel to the DMI exchange field[5].

Remarkably, the SAF racetracks exhibit an entirely distinct behaviour with regard to the dependence of DW velocity on H_x that depends on the degree of magnetization compensation (Fig. 3c–e). When poorly compensated, the field dependence is similar to that of the single-layer and SF structures (Fig. 3c). When the compensation is large enough (Fig. 3d,e), the field dependence of v shows a completely different behaviour in which the DW velocity is decreased for both positive and negative H_x and the behaviour no longer significantly depends on the ↓↑ or ↑↓ DW configuration. This behaviour can be understood by extending the 1D model of current- and field-induced DW dynamics to the SAF and SF structures (see Methods and Supplementary Discussions 1 and 2).

Finally, we find that in SAF structures without any spin Hall torque, such as Co|Ni structures with Au underlayers (that is, here Au|Co|Ni|Co|Ru|Co|Ni|Co|TaN), the DWs always move in the direction of electron flow and at modest speeds are driven only by conventional volume spin transfer torque, as shown in Fig. 4. By replacing the Pt underlayer with Au or, as previously shown by introducing a Au dusting layer between the Pt underlayer and the magnetic layer[6], the chiral spin torque is eliminated.

In summary, we find that a novel chiral exchange-coupling torque drives DWs much more efficiently at much higher speeds in synthetic AF racetracks. Moreover, the closer the magnetization of the racetrack approaches zero, the faster the DWs move. This remarkable result is a significant advance towards the development of ultradense, high-performance and energy-efficient racetrack memory and other potential domain-wall-based devices.

Methods

Sample preparation and Kerr microscopy. The magnetic thin film samples used in this study were formed by magnetron sputter deposition on Si(100) wafers covered with ~250Å SiO_2. The LM was deposited on an underlayer of 20 TaN|15 Pt or 50 Ta|30 Au and the UM was capped with 50 TaN. Kerr microscopy was carried out using an EVICO system that was modified to allow for injection of current pulses into the microwires. Note that the Kerr contrast is much weaker for SAF structures due to the lower net magnetization. Because the magnitude of the Kerr signal is approximately proportional to M_R, it becomes increasingly difficult to image the DW motion as the SAF structure becomes more nearly magnetically compensated.

Extraction of M_L and M_U values from magnetic hysteresis loops. The values of M_L and M_U were obtained from magnetic hysteresis loops measured with superconducting quantum interference device magnetometry measurements along the easy axis (perpendicular to the blanket sample plane). The diamagnetic backgrounds arising from the Si/SiO_x substrate were subtracted from the measured magnetic moment hysteresis loops, and then the subtracted data were divided by the sample area. From these final loops, the magnetic moments per area, M_R and M_S, with magnetic fields of $H_z = 0$ and 2T, respectively, were obtained. As $M_L + M_U = M_S$ and $M_L - M_U = M_R$, we can extract $M_L = (M_R + M_S)/2$ and $M_U = (M_S - M_R)/2$.

1D model of magnetization dynamics. The 1D model is based on the Landau–Lifshitz–Gilbert equation of magnetization dynamics that includes the Zeeman and damping torques, the standard volume adiabatic and non-adiabatic spin transfer torques, the spin Hall torque and the DMI exchange field. We have extended this model here to include two sub-racetracks that are ferro- or antiferromagnetically exchange-coupled to each other. Stationary solutions of DW motion under current and H_x are found, while assuming that the DW profile is not changed during the

motion except for a change in the orientation of the azimuthal angle ψ that the in-plane component of magnetization makes with the x-direction (Fig. 1).

Received 18 August 2014; accepted 10 December 2014; published online 23 February 2015

References

1. Chappert, C., Fert, A. & Van Dau, F. N. The emergence of spin electronics in data storage. *Nature Mater.* **6,** 813–823 (2007).
2. Parkin, S. S. P. Shiftable magnetic shift register and method of using the same. US patent 6834005 (2004).
3. Parkin, S. S. P., Hayashi, M. & Thomas, L. Magnetic domain-wall racetrack memory. *Science* **320,** 190–194 (2008).
4. Meckler, S. *et al.* Real-space observation of a right-rotating inhomogeneous cycloidal spin spiral by spin-polarized scanning tunneling microscopy in a triple axes vector magnet. *Phys. Rev. Lett.* **103,** 157201 (2009).
5. Ryu, K.-S., Thomas, L., Yang, S.-H. & Parkin, S. S. P. Chiral spin torque at magnetic domain walls. *Nature Nanotech.* **8,** 527–533 (2013).
6. Ryu, K.-S., Yang, S.-H., Thomas, L. & Parkin, S. S. P. Chiral spin torque arising from proximity induced magnetization. *Nature Commun.* **5,** 3910 (2014).
7. Emori, S., Bauer, U., Ahn, S.-M., Martinez, E. & Beach, G. S. D. Current-driven dynamics of chiral ferromagnetic domain walls. *Nature Mater.* **12,** 611–616 (2013).
8. Parkin, S. S. P. *et al.* Magnetically engineered spintronic sensors and memory. *Proc. IEEE* **91,** 661–680 (2003).
9. Ralph, D. C. & Stiles, M. D. Spin transfer torques. *J. Magn. Magn. Mater.* **320,** 1190–1216 (2008).
10. Manchon, A. & Zhang, S. Theory of spin torque due to spin–orbit coupling. *Phys. Rev. B* **79,** 094422 (2009).
11. Kawahara, T., Ito, K., Takemura, R. & Ohno, H. Spin-transfer torque RAM technology: review and prospect. *Microelectron. Reliab.* **52,** 613–627 (2011).
12. Hayashi, M., Thomas, L., Moriya, R., Rettner, C. & Parkin, S. S. P. Current-controlled magnetic domain-wall nanowire shift register. *Science* **320,** 209–211 (2008).
13. Parkin, S. S. P., More, N. & Roche, K. P. Oscillations in exchange coupling and magnetoresistance in metallic superlattice structures: Co/Ru, Co/Cr and Fe/Cr. *Phys. Rev. Lett.* **64,** 2304–2307 (1990).
14. Parkin, S. S. P. & Mauri, D. Spin-engineering: direct determination of the RKKY far field range function in ruthenium. *Phys. Rev. B* **44,** 7131 (1991).
15. Ryu, K.-S., Thomas, L., Yang, S.-H. & Parkin, S. S. P. Current induced tilting of domain walls in high velocity motion along perpendicularly magnetized micron-sized Co/Ni/Co racetracks. *Appl. Phys. Exp.* **5,** 093006 (2012).
16. Dzyaloshinskii, I. E. Thermodynamic theory of weak ferromagnetism in antiferromagnetic substances. *Sov. Phys. JETP* **5,** 1259–1272 (1957).
17. Dzyaloshinskii, I. E. Theory of helicoidal structures in antiferromagnets. 1. Nonmetals. *Sov. Phys. JETP* **19,** 960–971 (1964).
18. Moriya, T. Anisotropic superexchange interaction and weak ferromagnetism. *Phys. Rev.* **120,** 91–98 (1960).
19. Heide, M., Bihlmayer, G. & Blügel, S. Dzyaloshinskii–Moriya interaction accounting for the orientation of magnetic domains in ultrathin films: Fe/W (110). *Phys. Rev. B* **78,** 140403 (2008).
20. Thiaville, A., Rohart, S., Jue, E., Cros, V. & Fert, A. Dynamics of Dzyaloshinskii domain walls in ultrathin magnetic films. *Europhys. Lett.* **100,** 57002 (2012).
21. Hirsch, J. E. Spin Hall effect. *Phys. Rev. Lett.* **83,** 1834–1837 (1999).
22. Zhang, S. Spin Hall effect in the presence of spin diffusion. *Phys. Rev. Lett.* **85,** 393–396 (2000).
23. Liu, L., Lee, O. J., Gudmundsen, T. J., Ralph, D. C. & Buhrman, R. A. Current-induced switching of perpendicularly magnetized magnetic layers using spin torque from the spin Hall effect. *Phys. Rev. Lett.* **109,** 096602 (2012).
24. Khvalkovskiy, A. V. *et al.* Matching domain wall configuration and spin–orbit torques for very efficient domain-wall motion. *Phys. Rev. B* **87,** 020402(R) (2013).
25. Miron, I. M. *et al.* Fast current-induced domain-wall motion controlled by the Rashba effect. *Nature Mater.* **10,** 419–423 (2011).
26. Malozemoff, A. P. & Slonczewski, J. C. *Magnetic Domain Walls in Bubble Material* (Academic, 1979).
27. Ghosh, A., Auffret, S., Ebels, U. & Bailey, W. E. Penetration depth of transverse spin current in ultrathin ferromagnets. *Phys. Rev. Lett.* **109,** 127202 (2012).
28. Nonoguchi, S., Nomura, T. & Kimura, T. Longitudinal and transverse spin current absorptions in a lateral spin-valve structure. *Phys. Rev. B* **86,** 104417 (2012).
29. Zhang, J., Levy, P. M., Zhang, S. & Antropov, V. Identification of transverse spin currents in noncollinear magnetic structures. *Phys. Rev. Lett.* **93,** 256602 (2004).
30. Yakata, S., Ando, Y., Miyazaki, T. & Mizukami, S. Temperature dependences of spin-diffusion lengths of Cu and Ru layers. *Jpn J. Appl. Phys.* **45,** 3892 (2006).

Acknowledgements

The authors acknowledge partial support from the Army Research Office (contract no. W911NF-13-1-0107).

Author contributions

S.P. conceived and designed the experiments. K.R. carried out the experiment and analysed the experimental data. S.Y. grew films, patterned the devices and developed the 1D model. S.Y. and S.P. wrote the manuscript. All authors discussed the results and commented on the manuscript.

Additional information

Supplementary information is available in the online version of the paper. Reprints and permissions information is available online at www.nature.com/reprints. Correspondence and requests for materials should be addressed to S.P.

Competing financial interests

The authors declare no competing financial interests.